BBA - Proteins and Proteomics 1868 (2020) 140533

Contents lists available at ScienceDirect

BBA - Proteins and Proteomics

journal homepage: www.elsevier.com/locate/bbapap

Functional and structural characterization of an α-L-arabinofuranosidase from *Thermothielavioides terrestris* and its exquisite domain-swapped β-propeller fold crystal packing

Suelen Camargo[a,1], Evandro J. Mulinari[a,1], Leonardo R. de Almeida[a,1], Amanda Bernardes[a], Rolf A. Prade[b], Wanius Garcia[c], Fernando Segato[d], João R.C. Muniz[a,*]

[a] São Carlos Institute of Physics (IFSC), University of São Paulo (USP), São Carlos, SP, Brazil
[b] Department of Microbiology and Molecular Genetics, Oklahoma State University (OSU), Stillwater, OK, USA
[c] Centro de Ciências Naturais e Humanas, Universidade Federal do ABC (UFABC), Santo André, SP, Brazil
[d] Department of Biotechnology, Lorena School of Engineering, University of São Paulo (USP), Lorena, SP, Brazil

ARTICLE INFO

Keywords:
Thermothielavioides terrestris
α-L-arabinofuranosidase
Domain-swapping
GH62
*Tt*Abf62

ABSTRACT

The fungus *Thermothielavioides terrestris* plays an important role in the global carbon cycle with enzymes capable of degrading polysaccharides from biomass, therefore an attractive source of proteins to be investigated and understood. From cloning to a three-dimensional structure, we foster a deeper characterization of an α-L-arabinofuranosidase, a glycoside hydrolase from the family 62 (*Tt*Abf62), responsible to release arabinofuranose from non-reducing ends of polysaccharides. *Tt*Abf62 was tested with synthetic (*p*NP-Ara*f*) and polymeric substrates (arabinan and arabinoxylan), showing optimal temperature and pH (for *p*NP-Ara*f*) of 30 °C and 4.5–5.0, respectively. Kinetic parameters revealed different specific activity for the three substrates, with a higher affinity for *p*NP-Ara*f* (K_M: 4 ± 1 mM). The hydrolyzing activity of *Tt*Abf62 on sugarcane bagasse suggests high efficiency in the decomposition of arabinoxylan, abundant hemicellulose presented in the sugarcane cell wall. The crystal packing of *Tt*Abf62 reveals an exquisite domain swapping, located at the supramolecular arrangement through a disulfide bond. All crystallographic behaviors go against its monomeric state in solution, indicating a crystal-induced artifact. Structural information will form the basis for further studies aiming the development of optimized enzymatic properties to be used in biotechnological applications.

1. Introduction

The α-L-arabinofuranosidases (Abfs; EC 3.2.1.55) play a key role in the releasing process of L-arabinose from polysaccharides or arabino-oligosaccharides acting into α-(1 → 2)-, α-(1 → 3)- or α-(1 → 5)- linked L-arabinofuranosyl residues from the non-reducing end of poly- and oligosaccharides [1], increasing the hydrolysis of glycosidic bonds of polysaccharides by other enzymes [2]. According to the Carbohydrate-Active Enzymes database (CAZy; www.cazy.org), Abfs are grouped into six distinct families of glycoside hydrolases: GH2, GH3, GH5, GH39, GH43, GH51, GH54, and GH62 [3–5]. Based on their amino acid sequences, members of GH62 family has been divided into GH62_1 and GH62_2 subfamilies [6]. Additionally, the Abf families are further classified into three types based on divergence among themselves concerning substrates specificity [7,8].

These enzymes can release arabinose from many substrates and they are part of the xylanolytic system, being essential to disrupt arabinoxylan bonds [1,9]. Therefore, Abfs are of remarkably biotechnological importance [1], which extends from the use in industries oriented to agriculture [10], food [11], and also in cocktails for digestion of animal feed [10], enhancement of wines flavor [10,12], improvement in the clarification of fruit juices [10,13], and for the delignification of cellulose on biofuels production [14,15].

The filamentous fungus *Thermothielavioides terrestris* (previously *Thielavia terrestris*), belongs to the Ascomycota phylum and is among a limited number of eukaryotic species classified as thermophiles showing optimal growth above 45 °C [16]. Many enzymes characterized from *T. terrestris*, such as cellulases and hemicellulases, have been shown attractive for biotechnological applications involving biomass hydrolysis due to its favorable catalytic and stability profiles [16–19].

* Corresponding author at: n 1100, Jardim Santa Angelina - CEP 13563-120, São Carlos, São Paulo, Brazil.
E-mail address: jrcmuniz@ifsc.usp.br (J.R.C. Muniz).
[1] Authors contributed equally to this manuscript.

https://doi.org/10.1016/j.bbapap.2020.140533
Received 19 April 2020; Received in revised form 25 July 2020; Accepted 12 August 2020
Available online 29 August 2020

Aiming to contribute towards a better comprehension of these classes of enzymes, in this study we describe an α-L-arabinofuranosidase from the thermophilic fungus *T. terrestris* (subfamily GH62_2; named here *Tt*Abf62). The biochemical characteristics of purified *Tt*Abf62 were determined using sugar beet arabinan (SBA), wheat arabinoxylan (WAX), and *p*NP-Ara*f* as substrates. Moreover, the results presented here allowed inferences to be drawn on the hydrolysis of SBA, WAX, and *p*NP-Ara*f* by *T. terrestris*. The biophysical and biochemical outcomes aim to promote a better understanding of its catalytic mechanism when degrading renewable biomass, making them potential candidates for biotechnological applications in the biofuel and food industries. Furthermore, structural analyzes revealed the presence of a domain-swapping, probably a crystallization artifact. However, this new and beautiful shape elegantly preserves the active site of the enzyme where the catalytic pocket was structurally conserved between the 5-bladed β-propeller fold and confers protein stability.

2. Methods

2.1. Fungus cultivation

The *T. terrestris strain* UAMH 3264 was purchased at Microfungus Collection of University of Alberta, Devonian Botanic Garden Edmonton. The fungus was maintained in Potato Dextrose Agar medium (Sigma-Aldrich), at 45 °C for 5 days and the resulting mycelium was used for further cultivation that was performed in 1 L of the minimal medium [20] containing: 50 mL of 20× Clutterbuck solution [21], 1 mL of a trace elements solution (100 mL *MilliQ*® water: 2.2 g of $ZnSO_4$, 1 g of H_3BO_3, 0.5 g of $MnCl_2.4H_2O$, 0.5 g of $FeSO_4.7H_2O$, 0.16 g of $CoCl_2.5H_2O$, 0.16 g of $CuSO_4.5H_2O$, 0.11 g of $Na_2MoO_4.4H_2O$ and 5 g of Na_2EDTA at pH 6.5) and supplemented with 5 mM glutamine and 2.4 μM thiamine at pH 5.0 [22] using a rotary shaker (150 rpm) at 45 °C for 48 h.

2.2. Cloning, heterologous expression, and purification of TtAbf62

A total of 10 mg of the mycelium of *T. terrestris* was frozen in liquid nitrogen and then triturated using a pistil, placed in a 1.5 mL tube where 600 μL and the protocol for genomic DNA isolation was followed according to Damásio and collaborators [23]. To confirm the quality of the extracted DNA, the sample was analyzed on agarose gel (0.8%) by using the technique of electrophoresis.

The gene encoding the *Tt*Abf62 protein (GenBank: AEO64662.1) was amplified from *T. terrestris* genomic DNA by Polymerase Chain Reaction (PCR) and cloned into pETTrx-1-a/LIC expression vector (Novagen) allowing the expression of recombinant protein with a His_6-Thioredoxin-tag (His_6-Trx-tag) fused at its N-terminal [24,25] using specific oligonucleotides (Supplemental SM1). The vector containing the gene fragment of interest was transformed into *E. coli* Rosetta-gami™ 2 (DE3) (Novagen) expression system and the positive colonies were selected based on its resistance of growing in the presence of kanamycin and chloramphenicol. The recombinant *Tt*Abf62 was overexpressed in a 2 L Erlenmeyer containing 1 L of auto-induction medium (Supplemental SM2) added with kanamycin (0.05 $mg.mL^{-1}$) and chloramphenicol (0.036 $mg.mL^{-1}$), incubated in an orbital shaker with 150 rpm at 37 °C until an optical density of 0.6 at 600 nm; then the temperature was lowered and stabilized at 17 °C to induce protein expression for 17 h. The expression was monitored by SDS-PAGE. Cells were separated by centrifugation at 4500 x*g* for 20 min at 4 °C, and the pellet stored at −80 °C.

The pellet was resuspended in buffer A (50 mM Tris-HCl at pH 7.5, 150 mM NaCl and 10% (*w/v*) of glycerol) for cell disruption. The treated pellet was sonicated on ice in 3 cycles (30 s sonication, 30 s rest), in a sonicator (Fisher Scientific™ Model 505 Sonic Dismembrator) set with 45% amplitude. The lysate was then centrifuged at 14,000 x*g* at 4 °C for 40 min. Immobilized metal affinity chromatography (IMAC) with 2 mL Ni Sepharose 6 Fast Flow (GE Healthcare Life Sciences) was performed as the first purification step and after washing the column with buffer A, the recombinant protein was eluted with the same buffer with 150 mM imidazole added on it. Eluted solution was dialyzed overnight at 4 °C with buffer A. TEV protease (1:50 mg) was used for cleavage of the N-terminal His_6-Trx-tag. The second purification step repeats the IMAC purification step but elutes the protein with 20 mL of buffer A without imidazole. A third purification step was performed using size exclusion chromatography (SEC) on a HiLoad 16/60 Superdex 200 column (GE Healthcare Life Sciences) with buffer A. The purity of the recombinant protein was monitored by SDS-PAGE.

2.3. Biochemical characterization

Optimal pH for *Tt*Abf62 was determined by measuring the release of 4-nitrophenol from *p*-nitrophenyl-α-L-arabinofuranoside (*p*NP-Ara*f*; 2 mM; Sigma-Aldrich) as the substrate in 100 μL reactions containing 10 μg of the purified enzyme, and 50 mM McIlvaine buffer [26] with the pH ranging from 2.0 to 8.0 at 50 °C for 10 min. The optimal temperature was evaluated as described before, using the optimal pH varying the temperature from 10.0 to 60.0 °C, incubated for 15 min. After incubation, all reactions were quenched by the addition of 100 μL of a stop reagent (saturated sodium tetraborate solution) and the absorbances of the released *p*-nitrophenol was measured at 410 nm. For kinetic parameters determination, the end-point velocities of the enzymes were measured in 50 mM McIlvaine buffer at optimal pH and temperature, using *p*NP-Ara*f* in concentrations ranging from 0.1 to 50.0 mM, sugar beet arabinan (SBA) and wheat arabinoxylan (WAX) (Megazyme) in concentrations ranging from 1 to 27 $mg.mL^{-1}$ for 25 min for polysaccharides and 7 min for *p*NP-Ara*f*. All reactions were carried out in 100 μL and using 2 μg of the enzyme. The reducing sugars released in enzymatic reactions with polysaccharides was measured by the 3,5-dinitrosalicylic acid method (DNS) by measuring the absorbances at 540 nm [27]. The kinetics parameters (K_M and k_{cat}) were estimated by using direct weighting nonlinear least-squares regression analysis with Origin software (version 2018). The adjusted R-Square (Adj. R-Square) value was determined as a measure of the goodness of fit of experimental data. A calibration curve for the DNS method was plotted and used to calculate the amount of non-reducing end released. The 4-nitrophenol (*p*NP) was used to calculate the amount of arabinose released in *p*NP-Ara*f* reactions. All assays were carried out in triplicate and the averaged values reported.

The activity of *Tt*Abf62 in the presence of sugarcane bagasse *in natura* was evaluated by incubating the reaction in the agitation of 150 rpm in a rotatory shaker at 50 °C for 20 h. The duplicate reaction with 1.25 mL contained 20 mg of sugarcane bagasse *in natura* in 1.25 mL reaction with 40 mM McIlvaine buffer pH 4.5, 30 μg *Tt*Abf62 and 0.02% sodium azide. In the enzyme-free reaction (control), the volume corresponding to the enzyme was replaced by 50 mM Tris-HCl at pH 8.0 (stock buffer). The reaction was centrifuged at 13,000 x*g*, aliquoted in 100 μL, and the amount of reducing sugars was measured by DNS [27]. The thermal stability of *Tt*Abf62 was evaluated by measuring the residual activity at optimal pH and incubating the enzyme in temperatures of 30 and 50 °C. Amounts corresponding to 10 μg of the enzyme were aliquoted at time intervals and assays carried out using *p*NP-Ara*f* (0.5 mM final concentration) as the substrate in 100 μL reactions up to the total time of 36 h of incubation. All measurements were performed in triplicates and conducted in a 96-well microplate (Greiner) by using a Spectramax Plus 384 spectrophotometer (Molecular Device).

2.4. Thermal denaturation analysis

2.4.1. Differential scanning fluorimetry (DSF)

The DSF method was used to evaluate the structural integrity of *Tt*Abf62 in different conditions including a variety of buffer salts and

pH values. A CFX96 Real-Time System® (Bio-Rad) was used to detect the dye fluorescence allowing the determination of *Tt*Abf62 melting temperature T_m [28]. The assay was carried out applying 30 μg of purified *Tt*Abf62 to a 96 well plate containing different buffer solutions (Supplementary Table A.1), in a final concentration of 50 mM and 1:2000 of SYPRO Orange (Molecular Probes) and analysis were performed within the temperature range from 25 to 90 °C (with 1 °C increment of each 30 s). The fluorescence variation of SYPRO Orange was measured using excitation at 490 nm and emission at 530 nm. The construction and analysis of the curves, including the determination of the T_m of each sample, were carried out using Origin, version 2018 (OriginLab Corporation).

2.4.2. Circular dichroism (CD) spectroscopy

CD transition curve of *Tt*Abf62 was obtained using a JASCO J-815 CD spectropolarimeter in 50 mM McIlvaine, pH 4.5, and 50 mM Tris-HCl, 0.3 M NaCl, pH 7.5 buffers, using a 0.1 cm quartz cuvette, monitoring the ellipticity at 220 nm from 20 °C to 80 °C at a heating rate of 1 °C/min.

2.5. Protein crystallization, data collection, and processing

Crystals of *Tt*Abf62 were obtained using the purified protein in a concentration of 20 $mg.mL^{-1}$ in previously described buffer A. The protein concentration was determined by NanoDrop® 2000 spectrophotometer (Thermo Scientific). The initial screening of crystallization conditions was performed using a Crystal Gryphon LCP® crystallization robot (Art Robbins Instruments). Crystals were obtained after 30 days during exposure to 0.1 M sodium acetate (pH 4.6) and 2 M ammonium sulfate as reservoir solution at 18 °C.

The crystal diffraction and data collection were performed at the synchrotron radiation source at the Brazilian National Laboratory of Synchrotron Light from National Center for Energy and Materials (LNLS-CNPEM, Brazil). Diffraction datasets from the *Tt*Abf62 crystal were collected on beamline W01-MX2 using a PILATUS2M detector (Dectris). The data-collection strategy was determined using the iMosflm Strategy function [29], targeting > 95% completeness for data set collected to the given resolutions. The data were indexed and integrated using the programs XIA2 [30] and XDS [31] and scaled using Aimless [32,33] from the CCP4 suite [34]. The data completeness and $CC_{1/2}$ were used to determine the resolution limit.

2.6. Structure determination and refinement

Structure of *Tt*Abf62 was initially solved using molecular replacement with Phaser program [35]. The structure of a thermostable family GH62 α-L-arabinofuranosidase from *Streptomyces thermoviolaceus* (PDB id; 4O8N) [2] was used as a search model (79% of sequence identity). Crystallographic refinement was carried out using REFMAC5 [36] and manual model building was performed with Coot program [37] using weighted $2F_{obs} - F_{calc}$ and $F_{obs} - F_{calc}$ electron-density maps. Water molecules and additional fortuitous ligands such as sulfate ions and ethylene glycol molecules were manually placed appropriately by using Coot. The behavior of R_{work} and R_{free} was used as the main criteria to validate the refinement protocol and its convergence. The stereochemical quality of the model was evaluated with the MolProbity program [38]. The PISA server [39] was applied to verify oligomeric states by evaluating interfaces and their strength of the interaction between neighboring monomers generated by applying symmetry to the input file coordinates on the macromolecular assembly of *Tt*Abf62, consequently, predict the most likely biological form of the structure established through domain swapping.

2.7. Size exclusion chromatography with multiangle light scattering (SEC-MALS)

Using Waters 600 HPLC coupled to a Wyatt DAWN EOS light scattering instrument, Wyatt Optilab refractometer and Wyatt dynamic light scattering module (Wyatt Technology Corp., Santa Barbara, CA), SEC-MALS experiments were employed for chromatographic separations to verify the oligomeric state of *Tt*Abf62 using a Superdex 75 10/300 GL (GE Healthcare Life Sciences) equilibrated with 20 mM Tris-HCl at pH 8.0 and 300 mM NaCl buffer, with an eluent flow rate of 0.5 $mL.min^{-1}$. Molecular mass calculations were performed by ASTRA software.

2.8. Glutaraldehyde cross-linking

Glutaraldehyde treatment with cross-linkers was performed in 20 mM HEPES at pH 8.5. Reaction mix containing 1 μg of protein (control and *Tt*Abf62) in a total volume of 100 μL were treated with 5 and 10 μL of 2.3% freshly prepared solution of glutaraldehyde for 5 min at 37 °C. The reaction was stopped by the addition of 10 μL of 1 M Tris-HCl at pH 8.5. Cross-linked proteins were solubilized by the addition of an equal volume of Laemmli buffer [40], and verified by SDS-PAGE [41].

3. Results and discussion

3.1. Expression and purification of TtAbf62

The *Tt*Abf62 gene was localized in *T. terrestris* chromosome I between positions 9,454,228 and 9,455,223 at the complement strand. The gene sequence did not present introns and showed a region of 78 bp that correspond to the signal peptide (SP) in the *Tt*Abf62 protein. To oligonucleotides synthesis, the SP region was not considered and the gene showing 903 bp was amplified by PCR, cloned and expressed. The recombinant *Tt*Abf62 was expressed in *E. coli* system containing a tag of 6 histidine residues (His_6) and a thioredoxin (Trx) fused-protein. The total protein yield was approximately 2 $mg.L^{-1}$ of culture medium. Before TEV protease treatment, the SDS-PAGE analysis revealed a molecular mass bellow 45 kDa, which was consistent with the product of cloning on pETTrx-1-a/LIC (Fig. 1). After TEV cleavage the final molecular mass was around 31 kDa, which contains the residual site of TEV, plus one methionine, resulting in a molecular mass calculated from the mature amino acid sequence of 32.8 kDa (**Fig. 1**).

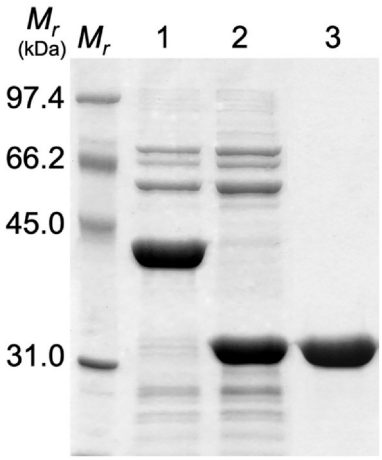

Fig. 1. Purification of *Tt*Abf62. M_r – molecular mass; 1 –*Tt*Abf62 after an IMAC step of purification (43 kDa); 2 – The protein with approximately 33 kDa after cleavage with TEV protease; 3 – Purified protein after size exclusion chromatography.

3.2. Thermal denaturation analysis

To investigate the thermostability under miscellaneous buffer conditions, the DSF was performed for *Tt*Abf62 and its melting point temperatures (T_m), at different buffering conditions, were determined, as shown in the Supplementary Table A.1. An overview of the analyzed conditions indicates that the higher T_m was 64 °C in 50 mM Bis-Tris buffer at pH 6.7. These results also demonstrated a reasonable thermal tolerance at temperatures near to 60 °C, decreasing the values of T_m only when the buffer pH was extremely acidic or alkaline regardless of the composition (more details in the Supplementary Table A.1).

The DSF analyses established that Bis-Tris buffer at pH 6.7 was the best condition for protein stability with a T_m of 64 °C, followed by the same buffer at pH 6.0 and Tris-HCl buffer at pH 7.5, both with a T_m of 63 °C. The addition of NaCl did not affect the T_m. Thermal denaturation was also examined by CD as a complementary technique providing additional information on T_m. Both CD conditions resulted in T_m values of 59.7 ± 0.4 and 62.6 ± 0.2 °C for McIlvaine and Tris buffers, respectively (Supplementary Fig. A.1). These data suggest that the enzyme has great structural stability over a wide spectrum of pH values and buffers conditions.

Considering that increased thermal stability of the enzyme is correlated with enhanced structural arrangement often followed by conformational integrity of protein [42–44], the crystallization tests of *Tt*Abf62 were performed in Tris-HCl buffer at pH 7.5, one of the best conditions pointed out by the DSF experiment.

3.3. Biochemical characterization

3.3.1. Optimum pH and temperature for TtAbf62 activity

Some enzymes of family GH62 can hydrolyze the substrate *p*NP-Ara*f*, and also display arabinofuranosidase activity when assayed with polymeric substrates [2,45,46]. The activity of *Tt*Abf62 was verified on polymeric substrates (Supplementary Fig. A.2) and did not show activity in the synthetic substrates as *p*-nitrophenyl-β-D-mannopyranoside, *p*-nitrophenyl-β-D-glucopyranoside, *p*-nitrophenyl-β-D-galactopyranoside, *p*-nitrophenyl-β-D-xylopyranoside (data not shown) although only against *p*NP-Ara*f* the activity was detected and applied to further analysis. The activity on arabinoxylan and arabinan reveals its capacity to release arabinose from the branches of water-soluble α-L-Ara*f*-(1 → 3) and α-L-Ara*f*-(1 → 2) bonds [47]. Beyond arabinoxylan, it is important to note that the enzymatic activity in branched arabinan, which contains a backbone of (1 → 5)-α-L-Ara*f* linkage, shows that *Tt*Abf62 may be acting in both polysaccharides from hemicellulose and pectin of sugarcane cell wall sources. The preference of the enzyme to hydrolyze substrates decorated with Ara*f*-α-(1 → 3) and Ara*f*-α-(1 → 2) bonds is clear since the significant activity is observed for WAX, indicating that the arabinosyl side chain is critical for the substrate recognition [48], making it plausible to classify the enzyme as arabinoxylan arabinofuranohydrolases [49].

*Tt*Abf62 exhibits high activity for *p*NP-Ara*f* over the pH range from 4.5 to 5.0 (Fig. 2a), with an abrupt decrease in its catalytic strength for pH values lower than 4.0 and over 5.0, suggesting an activity sensitive to pH. Since the DSF results pointed high structural stability for *Tt*Abf62 towards pH changes, the decrease in the enzyme activity should not be related with the loss in structural stability, but probably due to an impact on the overall charge of the amino acid residues involved in its activity.

When analyzed the optimal temperature of activity the highest values are in a range between 25 and 35 °C (Fig. 2b). Even being a thermophilic fungus, these values are compatible with the optimum pH and temperature previously observed for GH62 family towards *p*NP-Ara*f* as a substrate, e.g.: *Podospora anserina* pH 5.0 and 37 °C [6]; *Ustilago maydis* pH 5.0 and 37 °C [6] (Table 2).

Furthermore, the enzyme stability was assessed by measuring the residual activity after prolonged periods (up to 36 h) of incubation at 30 and 50 °C (Supplementary Fig. A.3). At 50 °C, the enzyme maintained a residual activity of 30.6% after 36 h, and in the same period, the residual activity at 30 °C was 43.5%. Even at the higher temperature tested (50 °C), the enzymatic activity demonstrated that the *Tt*Abf62 tolerates this condition for extended periods, whereas the complete inactivation was not observed, also the complete inactivation at 30 °C was not observed as well.

3.3.2. Kinetic parameters

The kinetic parameters were determined on substrates with all Adj. R-square greater than 0.95 where *Tt*Abf62 had the uppermost activity based on the substrate panel: *p*NP-Ara*f*, WAX and SBA (Table 1). As described in Table 1 equivalent values of k_{cat} was achieved for the substrates SBA (with a K_M = 9 ± 3 mg.mL^{-1}) and *p*NP-Ara*f* (K_M = 4 ± 1 mM^{-1}), wherein the *Tt*Abf62 shows higher affinity by *p*NP-Ara*f*, as well as other enzymes previously characterized. Comparing k_{cat} towards arabinan 5.8 ± 0.8 s^{-1}, and *p*NP-Ara*f* 6.8 ± 0.3 s^{-1}, the turnover number is in the same order of magnitude, suggesting the similar conversions rate independently of the polymeric or synthetic substrate. Nevertheless, the enzymatic preference (k_{cat}/K_M) is higher for *p*NP-Ara*f* when compared to SBA, whereas *Sth*Abf62A, *An*Abf62A and *Sc*Abf62A (Table 1) prefer WAX. *Tt*Abf62 also presented the highest catalytic efficiency and enzymatic activity (U mg^{-1}) in *p*NP-Ara*f* and SBA when compared to other enzymes as described in Table 1.

The activity towards *p*NP-Ara*f* can be explained by the insights from the structural analysis of the *Tt*Abf62 (section 3.4), which has the catalytic triad composed of two aspartates (Asp58 and Asp165) and one glutamate (Glu217) coordinating the substrate. Also, the residues Asp58 and Asp165 are acting as catalytic residues, interacting with a *p*-nitrophenolate ring that stabilizes the intermolecular interactions.

3.3.3. Activity of TtAbf62 in sugarcane bagasse

The sugarcane cell wall contains 40% arabinoxylan (AX), where arabinoside side chain may cause a steric hindrance for xylanases [55]. The hydrolysis with *Tt*Abf62 was qualitatively tested against natural biomass to estimate the potential of this enzyme to act on complex substrates. Evaluated by DNS method [27], the addition of *Tt*Abf62 resulted in a higher concentration of reducing terminals (4.5 μmol glucose equivalent), compared with the enzymatic cocktail itself (0.2 μmol glucose equivalent). This might be related to its ability to remove arabinose side chains from the AX, as well as arabinan, decreasing steric restraint in branched polysaccharides, making it more susceptible to hydrolysis by exo and endoxylanases.

3.4. Structural characterization

3.4.1. Overall structure

After the crystallization process, orthorhombic crystals of *Tt*Abf62 were obtained (*I*222; a = 75.267 Å, b = 79.747 Å, c = 82.922 Å) and diffracted up to 1.87 Å resolution. The structure was determined by molecular replacement with one molecule in the asymmetric unit. The protein chain was comprised of 303 amino acid residues (from Gly28 to Arg331), two ions: calcium (Ca^{2+}), sulfate (SO_4^{2-}), and one molecule of ethylene glycol (EDO). All amino acids and ligands built in the structure exhibited a well-defined electron density. Final crystallographic R_{work} and R_{free} values were 14.7% and 19.5%, respectively, with more than 96% of the residues located on the sterically allowed regions of the Ramachandran plot. Further refinement statistics are described in Table 2.

The *Tt*Abf62 asymmetric unit is shown in Fig. 3a. The N-terminus began in a loop from Gly28 to Thr54 residue, followed by five β-sheets (called blades I to V), usually composed of four antiparallel β-strands. Blades I, II, and III are composed of four antiparallel β-strands; blade IV by five mixed β-strands plus a η4 helix; and blade V by three antiparallel β-strands, respectively, forming a set of 20 β-strand, from β1 to β20, linked by loops with variant lengths. Also, five helices (called η1 to

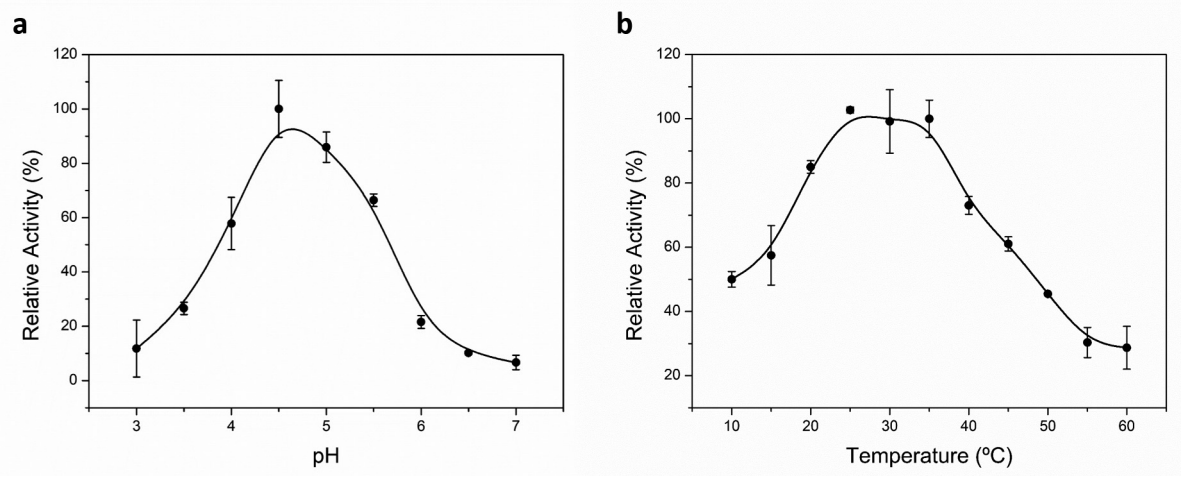

Fig. 2. Optimal pH and temperature of *Tt*Abf62 for *p*NP-Ara*f*. In both cases (a) and (b), the solid line is just a guide for the eye.

Table 1
Kinetic parameters of *Tt*Abf62. Substrate specificity and kinetic data of GH62 enzymes with known structure deposited on PDB. pNP: para-nitrophenol, *p*NP-Ara*f*: para-nitrophenyl α-L-arabinofuranoside, *p*NP-X: para-nitrophenyl β-D-xylopyranoside, *p*NP-Ara*p*: *p*NP-α-L-arabinopyranoside, SBA: sugar beet arabinan, WAX: wheat arabinoxylan, HV: high viscosity, LV: low viscosity. Sp. act.: Specific activity, U: unit defined as the release of 1 μmol of product per min per mg of the substrate under the specific assay conditions. *values are normalized according to the unit.

Source, (protein ID), accession no.	Assay conditions, substrate	Activity	K_M	k_{cat}	k_{cat}/K_M	Reference
Thermothielavioides terrestris (*Tt*Abf62), AEO64662.1	pH 4.5, 30 °C	Sp. Act ($U\ mg^{-1}$)	mM	s^{-1}	$s^{-1}.mM^{-1}$	This study
	*p*NP-Ara*f*	0.78	4 ± 1 $mg.mL^{-1}$	6.8 ± 0.3 s^{-1}	2 $s^{-1}.mg^{-1}.mL$	
	WAX	0.12				
	SBA	0.21	9 ± 3	5.8 ± 0.8	0.6	
Streptomyces coelicolor A3 (*Sc*Abf62A), CAA16189.1	pH 5.5, 30 °C		mM	s^{-1}*	$s^{-1}.mM^{-1}$*	[46]
	*p*NP-Ara*f*		1.9 $mg.mL^{-1}$	0.02 s^{-1}	0.01 $s^{-1}.mg^{-1}.mL$	
	WAX		7.3	0.30	0.04	
Podospora anserina S mat+ (*Pa*Abf62A), CAP62336.1	pH 5.0, 37 °C	Sp. Act ($U\ mg^{-1}$)	mM	s^{-1}*	$s^{-1}.mM^{-1}$*	[a] [6];[b] [50];
	*p*NP-Ara*f*	0.61[a] 0.38[b]	6.1[a,b]	0.38[a,b]	0.06[a,b]	
	WAX-LV	1[b]				
	SBA	0 .11[b]				
Streptomyces thermoviolaceus OPC-520 (*Sth*Abf62A-m2,3), BAB84113.1	pH 7.0, 55 °C	Sp. Act ($U\ mg^{-1}$)*	mM	s^{-1}	s^{-1} mM	[2,51]
	*p*NP-Ara*f*	0.003	3	1.3	0.5	
	*p*NP-X	$7.8{\cdot}10^{-6}$				
	*p*NP-Ara*p*	$5.2{\cdot}10^{-7}$	8.2 $mg.mL^{-1}$	0.01 s^{-1}	0.001 $s^{-1}.mg^{-1}.mL$	
	WAX-HV	0.04	12	180	15	
	WAX-LV	0.02				
	SBA	0.001	32	6	0.2	
Ustilago maydis 521 (*Um*Abf62Am2,3), EAK85571.1	pH 5.0, 37 °C[a] pH 4.5, 40 °C[b]	Sp. Act ($U\ mg^{-1}$)	mM	s^{-1}*	$s^{-1}.mM^{-1}$*	[a] [6]; [b] [52]
	*p*NP-Ara*f*	0.06[a]; 0.012[b]	7.5[a]	0.04[a]	0.005[a]	
	WAX-LV	30[b]				
	SBA	0 .003[b]				
Aspergillus nidulans FGSC A4 (*An*Abf62A-m2,3), EAA59562.1	pH 5.5, 37 °C	Sp. Act ($U\ mg^{-1}$)			$s^{-1}.mM^{-1}$	[53]
	*p*NP-Ara*f*	1.6			0.26	
			$mg.mL^{-1}$	s^{-1}	$s^{-1}.mg^{-1}.mL$	
	WAX-LV	67	4.9	17 8	36	
Scytalidium thermophilum CBS 625.91 (*St*Abf62Cm2,3), AHZ56660.1	pH 7.0, 50 °C	Sp. Act ($U\ mg^{-1}$)				[47]
	*p*NP-Ara*f*	0.02				
			$mg.mL^{-1}$	s^{-1}	$s^{-1}.mg^{-1}.mL$	
	WAX-HV		3.66	0.28	0.07	
	SBA	1.5 ± 0.4				
Coprinopsis cinerea (*Cc*Abf62A), BAK14423.1	pH 7.0, 40 °C	Sp. Act ($U\ mg^{-1}$)*				[54]
	WAX	0.15				

Table 2
Data collection and refinement statistics. Values in parentheses are for the highest resolution shell.

Name	*Tt*Abf62 (PDB ID: 6CC7)
Data collection	
Beamline	W01A–MX2, LNLS
Wavelength (Å)	1.4586
Space group	*I*222
a, *b*, *c* (Å)	75.27, 79.75, 82.92
V_M[a] ($Å^3.Da^{-1}$)	1.79
Solvent content (%)	31.3
Resolution (Å)	33.05–1.87 (1.91–1.87)
Unique reflections	20,946 (1318)
Completeness (%)	99.8 (97.4)
Multiplicity	5.5 (2.8)
$CC_{1/2}$ (%)	99.8 (83.8)
R_{merge} (%)	7.1 (38.6)
R_{meas} (%)	8.4 (52.2)
$R_{p.i.m.}$ (%)	4.5 (34.9)
Mean $I/\sigma(I)$	11.9 (2.2)
Refinement	
Resolution (Å)	57.48–1.87
No. of reflections	19,767
Completeness (%)	99.65
R_{work} (%)	14.74
R_{free}[b] (%)	19.53
Average B factor ($Å^2$)	23.69
Protein	23.78
Waters	35.26
Metal	39.66
Inorganic	39.33
Organic	29.19
No. of protein atoms	2334
No. of solvent atoms	298
No. of molecules in the asymmetric unit	1
R.m.s.d.[b], bonds (Å)	0.014
R.m.s.d., angles (°)	1.628
Ramachandran plot	
Favored (%)	96.36
Allowed (%)	3.31
Outliers (%)	0.33
Clashscore	0.44
MolProbity score [38]	0.90

[a] Matthews coefficient.
[b] The test set uses ~5% of the data.

η5) are distributed along the chain (Fig. 3b).

Analysis using PISA server [39] showed that the opened interface adopted by the structure of *Tt*Abf62 allows contacts between chains related by a symmetry operation (−x + 1, y, −z) throughout 125 residues (41.3% of the whole structure). These interactions embrace a variety of hydrogen bonds, a salt bridge between His283A and Asp58B ($d_{ND1\text{-}OD1}$ = 3.10 Å), and also a disulfide bond between Cys32A (from chain A) and Cys300B (from chain B) with a distance $d_{S\text{-}S}$ of 2.03 Å. This interchain disulfide is connecting a loop (formed by residues 28 to 54) located at the N-terminus of chain A (Cys32A) and a η4 located at the C-terminus of chain B (Cys300) (Fig. 4).

The disulfide bond parameters are calculated according to the empirical formula described by Katz et al. [56] and Schmidt et al. [57] (https://services.mbi.ucla.edu/disulfide/). Interestingly, the presence of a disulfide bond summed with the opened interface adopted by the structure provided the possibility of an exquisite phenomenon of domain swapping, first observed in the GH62 family. This domain swapping generates an interface of contacts among neighbor protein chains involving blade I from chain B (blade IB) fitted onto chain A and blade I from chain A (blade IA) shuffled to chain B. Additionally, this phenomenon also relies on the so-called "molecular velcro", joining the N-terminal β1 in one of the modular β-sheets (β20) via hydrogen bonds [58]. However, in this particular case, the molecular velcro is arranged by hydrogen bonds connecting the loop (28–54) from N-terminal upon β20 from C-terminal (details in Supplementary Fig. A.4). As a result, the enzyme TtAbf62 adopts a homodimeric blade-swapped β-propeller fold (see scheme in Supplementary Fig. A.5), each part containing five blades (I to V) radially arranged in two pseudo-5-fold axes wherein the beta-sheets (β1 to β20) are repeated, as shown in Fig. 4a and Supplementary Fig. A.5, maintaining the catalytic residues on its appropriated position (Fig. 4b).

The domain swapping occurs when two or more molecules make a partial exchange of domains among their structures, usually to form oligomers, from their monomeric subunits [59–63]. It represents not only an isolated event of structural innovation but differently, these swaps enable the creation of new interfaces of interactions previously absent in the monomer or a closed arrangement [59]. Considered an important innovative aspect in the structure and function of a protein, even been commonly found, such a mechanism is still poorly understood structurally.

A search for similar structures of *Tt*Abf62 was performed using the Dali server [64] (Supplementary Table A.2) and the results are displayed as aligned sequences with graphical enhancements performed by ESPript 3.0 [65] (Supplementary Fig. A.6). Comparisons to similar structures from *Streptomyces coelicolor Sc*Abf62A (PDB ID 3WMY; 3WN0; 3WN1; 3WN2) [46], *S. thermoviolaceus Sth*Abf62A (PDB ID 4O8N; 4O8O and 4O8P) [2], *Podospora anserina Pa*Abf62A (PDB ID 4N4B and 4N2Z), *Ustilago maydis Um*Abf62A (PDB ID 4N1I and 4N2R) [6], *Aspergillus nidulans An*Abf62A (PDB ID 5UBJ) [9], *Scytalidium thermophilum Sth*Abf62C (PDB ID 4PVA and 4PVI) [47], *Coprinopsis cinerea Cc*Abf62A (PDB ID 5B6S) [66] and *Talaromyces pinophilus Tp*Abf62 (PDB ID 6F1J) [67].

3.4.2. Catalytic pocket description

In-depth analysis side-by-side of structurally characterized GH62 enzymes revealed that the catalytic triad [68]: an aspartate (acting as a general acid); glutamate (acting as a general base); and an aspartic acid supposedly modulating the pKa of the catalytic general acid, as observed in many crystallographic structures [2,6,46] and supported by site-directed mutagenesis and kinetic data [2,46], were also conserved in *Tt*Abf62, named Asp58 (from β1), Asp165 (from β9), and Glu217 (from β13) (Fig. 4b, Supplementary Table A.3, and Fig. A.4). These residues interact with the ligands similarly as described in *Sc*Abf62A (3WN0) [46], *Sth*Abf62A (4O8O) [2] and *Um*Abf62A (4N2R) [6] for an arabinose residue; in *Sth*Abf62A (4O8P) [2] for a xylotetraose residue; in *Sc*Abf62A (3WN1) [46] and *Sth*Abf62C (4PVI) [47] for xylotriose residues; in *Sc*Abf62A (3WN2) [46] for a xylohexaose residue; and in *Pa*Abf62A (4N2Z) [6] for a cellotriose residue. They are also conserved independently of their subclassification of the family, GH43, and GH62. For *Tt*Abf62 (6CC7), a molecule of ethylene glycol (EDO, from the crystallization condition) is observed at the catalytic site, interacting via hydrogen bonds directly with Lys57 ($d_{NZ\text{-}O1}$ = 2.84 Å) and Asp58 ($d_{OD2\text{-}O1}$ = 2.72 Å).

Alignments of the three-dimensional structures (Fig. 5) and amino acid sequences (Supplementary Fig. A.6) revealed that in the catalytic pocket, the residues at the position equivalent to 57 and 283 in *Tt*Abf62 (6CC7) are conserved in all structures, except in *Tp*Abf62 (6F1J), since the Lys57 and His283 were mutated by an arginine (Arg) and serine (Ser), respectively. The key residues at position 58 (acting as a general acid), position 125 and 165 (acting as a pKa modulator), position 217 (acting as a general base), and positions 307 and 317 are fully conserved in all available structures.

The calcium ions (Ca^{2+}) listed in Table A.3 are usually hydrogen-bonded to a histidine residue (Ca-His), equivalent to His283 (Supplementary Fig. A.6), with a few exceptions for *Tt*Abf62 (6CC7) and *Sth*Abf62C (4PVA and 4PVI). The presence of this histidine residue in the catalytic pocket has been proposed to be an asset in combination with the catalytic triad residues [47].

Some particular water molecules (H_2O) also appear to play a significant role in the catalytic site. In *Tt*Abf62, the H_2O 533, 542, 574, and 594 are present, and their equivalent positions in other structures

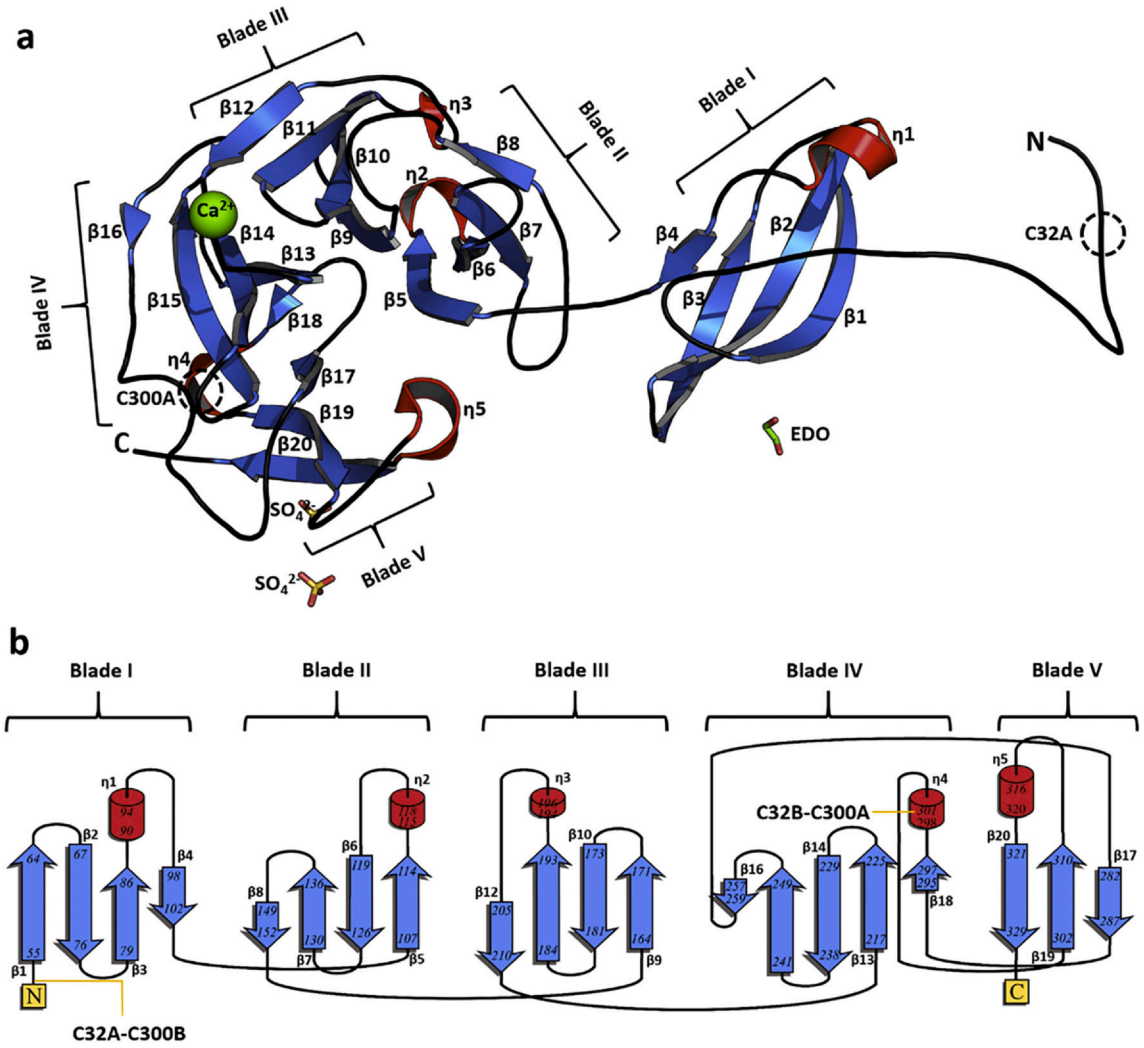

Fig. 3. Topology and top view of the asymmetric unit. a) The overall structure of *Tt*Abf62 revealing a five-bladed β-propeller fold, top view showing the numbering of 5 blades (blades I to V), a disulfide bond between Cys32A and Cys300B, an ethylene glycol (EDO) molecule located at partial catalytic cleft correspondent to channel of the fold, two sulfate ions (SO_4^{2-}) close to Blade V, and a calcium ion (Ca^{2+}) coordinated close to Blade IV. b) The overall topology of *Tt*Abf62 revealing a five-bladed β-propeller fold. Amino acid residue numbers are given at each start and end of the respective secondary structure elements, β-strands are indicated as arrows β1–β20 (shown in blue) and helices are indicated by cylinders η1–η5 (shown in red), respectively.

are often connected to the His283 (His-H_2O) as shown in 3WN1, 3WN2, 4PVI and 5B6S. The H_2O542 intermediates an interaction between residues Gln307 and Tyr317 (Gln-H_2O-Tyr), however, it was not observed in 3WN0 and 4N2R, where the water molecule is replaced by β-L-arabinofuranose, and for 5UBJ and 4PVA was replaced by a calcium and phosphate ion, respectively. The list of structural elements in the catalytic pocket for the Abfs GH62 family is presented in Supplementary Table A.3.

The calcium ion (Ca^{2+}) presented in the structure of *Tt*Abf62 is located in a completely different position when compared to other solved structures for the same family. In *Tt*Abf62 the Ca^{2+} is located at the interface of contacts between two dimeric arrangements, specifically by the residue Thr212 and (H_2O)730 both within 3.9 Å of distance as detailed in Supplementary Fig. A.7a. Furthermore, the chelation of Ca^{2+} by EDTA had no apparent effect on the enzymatic activity (data not shown). Fortuitous ligands from crystallization condition, the sulfate ions (SO_4^{2-}) 402 and 403 are coordinated on the surface of the structure by residues Trp91 and Asn312, respectively, with the addition of some water molecules (Supplementary Fig. A.7b-c).

3.4.3. Structural insights

According to CAZy, all the structures of characterized GH62 family share a high degree of similarity, adopting the β-propeller fold with five blades (I-V), and their active site is composed of previously highlighted catalytic triad [68], that often interacts with the substrate.

The structure of *Tt*Abf62 was compared to other Abfs belonging to the family GH62 in complex with xylooligosaccharides and revealed that their orientations were similar (Supplementary Fig. A.8). According to Maehara et al. [46], the residues Trp270 and Tyr461 in *Sc*Abf62A are interacting with xylotriose (PDB ID 3WN1) and xylohexaose (PDB ID 3WN2) ring at subsites +3NR and + 1, respectively. The same positions were found in *Tt*Abf62, corresponding to Trp126 and Tyr317, respectively. The residue Asn318 in *Tt*Abf62 (PDB ID 6CC7), also has the same orientation as described in the structures complexed with xylooligosaccharides: *Sc*Abf62A (PDB IDs 3WN1 and 3WN2) [46] with an equivalent position of Asn462; Asn339 in *Sth*Abf62C (PDB ID 4PVI) [47]; Asn321 in *Pa*Abf62A (PDB ID 4N2Z) [6]; and Asp350 in *Sth*Abf62A (PDB ID 4O8P) [2]. Amino acids at this position are usually involved in the hydrogen bond to subsite +2NR and reported as responsible for affecting the activity specifically in polysaccharides [46].

To demonstrate the most likely bio-assembly of *Tt*Abf62 in solution, SEC-MALS and cross-linking experiments were carried out. Differently of the crystal structure, assays with *Tt*Abf62 in solution demonstrate

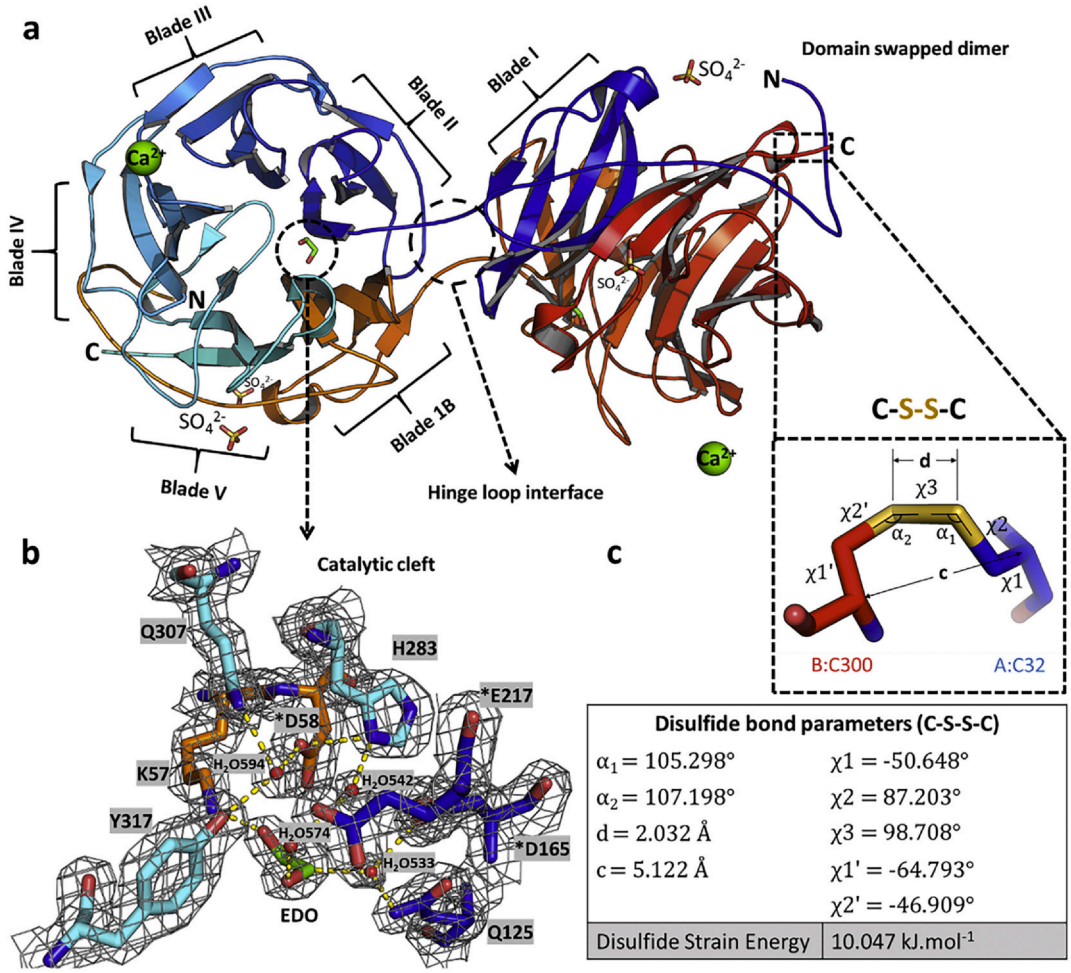

Fig. 4. Detailed view of the swapped domain from TtAbf62, its catalytic pocket, and disulfide bond. a) TtAbf62 represented as a homodimer through a domain swap. In detail, the N- (dark blue) and C- (dark red) terminus from their monomer chains respectively, which are connected via a disulfide bond. Five blades of β-strands can be observed assembling the dimeric system required for this structure. Calcium ions (Ca2+) are represented as spheres colored in green; sulfate ions (SO42−) and ethylene glycol (EDO) ligands can also be observed. b) Detailed view of the catalytic pocket with hydrogen bonds between water molecules mediating interactions to EDO and also a salt bridge evolving H283 and *D58 residues. Isomesh level 1.0. c) Detailed view of the disulfide bond between A:C32 (belonging to the N terminus) and B:C300 (belonging to the C terminus) with its respective parameters.

evidence of a monomeric arrangement, suggesting that a closed interface regarding all blades in a classical β-propeller fold is most reliable.

In general, the domain swapping phenomena has no clear explanations, and one possible reason could be due to specific conditions that the protein had been exposed [60]. These conditions can be justified through some processes such as pH and temperature changes, mutation, and denaturing agents [63,69]. Also, the physiological conditions of *T. terrestris* are at acidic pH and temperature of 45 °C [16], providing the basis to believe that the new molecular arrangement (dimeric) of the enzyme with domain swapping and the complement of catalytic pocket by surrounding molecule to be an artifact arising from molecular alterations caused by the environmental and physiological conditions during crystallization.

3.5. Size exclusion chromatography with multiangle light scattering (SEC-MALS) and glutaraldehyde cross-linking

When analyzed by SEC-MALS, *Tt*Abf62 exhibited a symmetrical peak with an average molecular mass of (32.1 ± 0.2) kDa (Fig. 6b). The expected theoretical molecular mass under denaturing conditions for *Tt*Abf62 is 32.8 kDa, which represents only 2% of error for the estimative mass. This result indicates that *Tt*Abf62 is likely a monomer in solution; despite the crystal structure has shown a possible homodimer or even a homotetramer (if considering the dimer-dimer interface for Ca^{2+}). According to Yang et al. [70], domain swapping happens at high protein concentration where a monomer becomes less favorable entropically and proteins tend to form homodimers. The exchanged blade generates an oligomerization in such matter to afford to rise in protein stability by providing additional contacts between chains [71]. Therefore, measurements of the molecular mass for a sample with higher protein concentration, close to the condition of the drop in the condition of crystallization were carried out. Thus, the graphs of Fig. 6b-c show two more concentrations: 2 $mg.mL^{-1}$ in buffer A and 54 $mg.mL^{-1}$ in 1:1 buffer A and crystallization solution, respectively, with both confirming the protein as a monomer in solution. Although there are small peaks with a mass of approximately (51 ± 1) and (52 ± 2) kDa, they do not correspond to another oligomeric state of *Tt*Abf62, but rather a contaminant not eliminated during the purification processes, as can be seen in the SDS-PAGE gel of Fig. 6a in two concentrations: 2 and 54 $mg.mL^{-1}$.

Moreover, *Tt*Abf62 was also analyzed by SDS-PAGE after glutaraldehyde cross-linking reaction, and again a single band corresponding a monomer predominates, indicating that *Tt*Abf62 does not form another oligomeric state in solution (Fig. 7). To conclude, *Tt*Abf62 is a monomer in solution, adopting a more compact structure like all other proteins from the GH62 family.

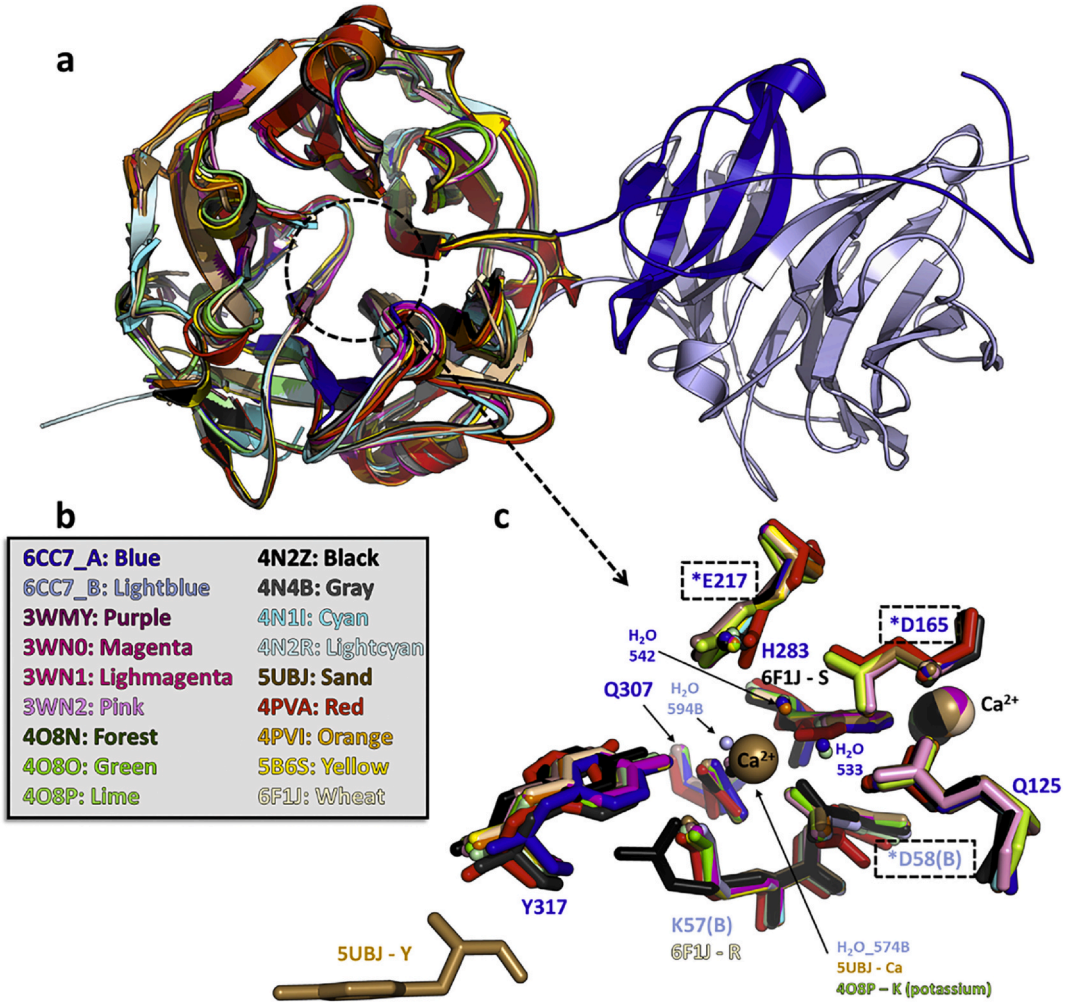

Fig. 5. Structural superposition of *Tt*Abf62 (6CC7) with representative Abf from the GH62 family with similar three-dimensional structures. a) Superimposition of representative Abf structures; b) Color scheme adopted for identification of the structures; c) Residues in the active site of similar Abf with their equivalent in *Tt*Abf62, represented by one letter code (colored as described in b). the catalytic residues *D165 and *E217 belong to chain A of *Tt*Abf62 and residue *D58 belongs to chain B of *Tt*Abf62, forming its catalytic site. Water molecules with structurally conserved positions are represented as small spheres (colored by chains and structure as described in b). Calcium ions (Ca^{2+}) are represented as spheres with arbitrary radii colored by chains. Residues are labeled by one-letter code. Additional structural comparisons of *Tt*Abf62A are summarized in Supplemental Table A.3.

4. Conclusion

The enzyme *Tt*Abf62 catalyzes the hydrolysis of arabinose residues of the arabinan branches, arabinoxylan as well as acts in sugarcane bagasse *in natura*, whereas, suggesting a great versatility of the fungal enzyme against the natural substrates, emerging its biotechnological potential. The structural differences assisted in the clarification of the reasons for these observed functional differences. Sequence alignments of glycoside hydrolase GH62 show conserved blocks. The catalytic pocket was structurally conserved between the 5-bladed-propeller fold. The β-propeller architecture followed a pattern, with the junction of C and N-terminus blades forming a pseudo-5-fold symmetry, which confers protein stability. This stability is also strengthened by disulfide bonds and the “non-classical molecular velcro”. The structural outcome for *Tt*Abf62 is unexpected, considering the predominant monomeric nature of the homologous proteins adopting classical β-propeller folds. Therefore, the possibility of evolution or mere crystallization artifact on protein oligomerization for this family of enzymes was shown. Such things may lead to its thermostability to be related to the folding. All analyses presented conclude that the quaternary structure of the enzyme *Tt*Abf62, in crystal, is in a dimeric arrangement, once the interdependence between the catalytic residues and domain-swapped (blade I) are necessary for complementarity, and it is only possible through this molecular architecture. Therefore, the domain swapping reveals a new structure within the GH62 family proteins and suggests a novel structural arrangement. The nature of this behavior may be related to the favorable entropic as a form of storage or compacting of the enzyme in high concentrations.

Author contributions

S.C., E.J.M., L.R.A., and J.R.C.M. designed the research. S.C. and E.J.M. purified *Tt*Abf62. L.R.A. and J.R.C.M. prepared cryo-crystals samples and collected datasets. S.C., E.J.M., A.B., and F.S. characterized *Tt*Abf62 enzymatically. W.G. characterized *Tt*Abf62 biophysically. L.R.A. and J.R.C.M. processed X-ray diffraction images and refined the atomic coordinates. S.C., E.J.M., L.R.A., R.P., and J.R.C.M. wrote the paper with support from all other authors.

Footnote

This article contains supplementary data: SM1, SM2, Table A.1, Table A.2, Table A.3, Fig. A.1, Fig. A.2, Fig. A.3, Fig. A.4, Fig. A.5, Fig. A.6, Fig. A.7, and Fig. A.8.

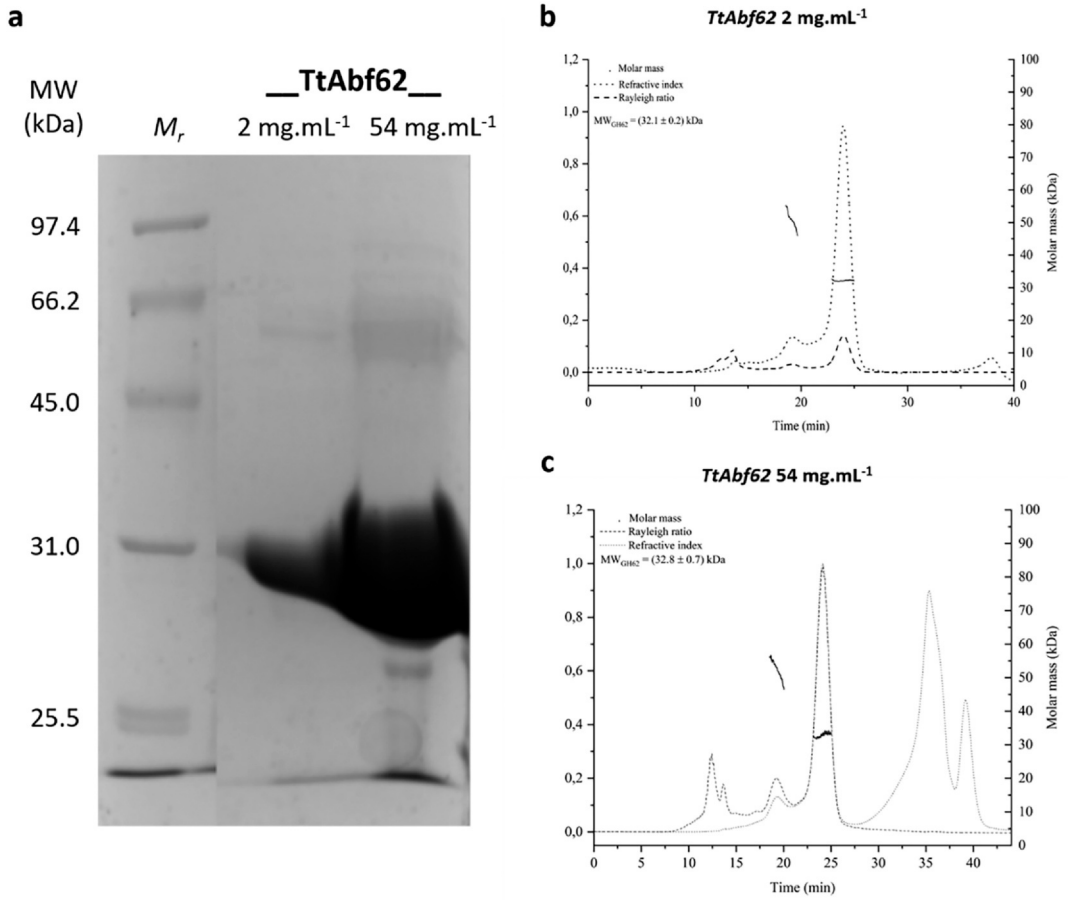

Fig. 6. Multiangle Light Scattering (SEC-MALS) analysis for different concentrations of *Tt*Abf62 in solution. a) 12% SDS-PAGE after SEC. M_r – molecular mass; lanes 2 and 3 show *Tt*Abf62 in two different concentrations: 2 and 54 mg.mL^{-1}, respectively. SEC-MALS of purified *Tt*Abf62 at 2 mg.mL^{-1} (b) and 54 mg.mL^{-1} (c). For all samples, the small peak represents a possible contaminant confirmed by SDS-PAGE (a) with the highest peak representing *Tt*Abf62 in the monomeric state in solution in agreement with the theoretical molar mass of 32.8 kDa. MALS calculations are dependent on a good estimate of the refractive index increment (dn/dc) of the sample, near to 0.185 for proteins [72]. The peaks in (b) correspond to (51 ± 1) and (32.1 ± 0.2) kDa, respectively; peaks in (c) correspond to (52 ± 2) and (32.8 ± 0.7) kDa, respectively.

The atomic coordinates and structure factors (code 6CC7) have been deposited in the Protein Data Bank, Research Collaboratory for Structural Bioinformatics, Rutgers University, New Brunswick, NJ (http://www.rcsb.org/).

Declaration of Competing Interest

All authors of this work declare that have no potential conflict of interest and that there is no financial, consultant, institutional or other relationships that might lead to bias or conflicts of interest in this research. Financial grants, infrastructure and fellowships supporting this

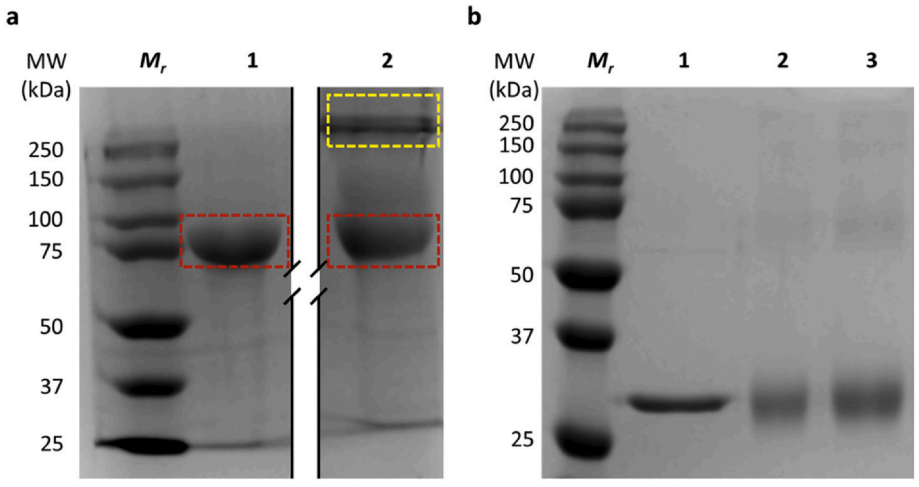

Fig. 7. Glutaraldehyde Cross-linking reaction. a) 10% SDS-PAGE of the reaction (positive control) using a known sample of a homodimer in solution; Mr – molecular mass reference; 1 – protein control of 84.9 kDa (monomeric, red box); 2 – after crosslink control reaction with 5 μL of glutaraldehyde mixture (dimers - yellow box and monomers - red box). b) 15% SDS-PAGE after reaction with TtAbf62. Mr molecular mass; 1 – only the purified protein. The TtAbf62 after crosslink reaction with 5 μL and 10 μL of glutaraldehyde mixture: lanes 2 and 3, respectively.

work are described below.

Acknowledgments

We would like to thank the National Synchrotron Light Laboratory (LNLS, Brazil); CNPEM – National Center for Research in Energy and Materials; São Paulo Research Foundation (FAPESP) for the financial support via grants # 2017/16291-5, 2014/50897-0 (JRCM), 2014/18714-2, 2017/50025-0, 2019/22284-7 (FS) and 2016/09152-6 (LRA); São Carlos Institute of Physics/University of Sao Paulo; Conselho Nacional de Desenvolvimento Científico e Tecnológico(CNPq) for the financial support via grant # 308865/2018-9 (JRCM) and 302627/2018-9 (FS); and Coordenação de Aperfeiçoamento de Pessoal de Nível Superior (CAPES) for fellowship to SC and EJM.

Appendix A. Supplementary data

Supplementary data to this article can be found online at https://doi.org/10.1016/j.bbapap.2020.140533.

References

[1] C. Wilkens, S. Andersen, C. Dumon, J.-G. Berrin, B. Svensson, GH62 arabinofuranosidases: structure, function and applications, Biotechnol. Adv. 35 (6) (2017) 792–804, https://doi.org/10.1016/j.biotechadv.2017.06.005.

[2] W. Wang, G. Mai-Gisondi, P.J. Stogios, A. Kaur, X. Xu, H. Cui, O. Turunen, A. Savchenko, E.R. Master, Elucidation of the molecular basis for arabinoxylan-debranching activity of a thermostable family GH62 alpha-l-arabinofuranosidase from *Streptomyces thermoviolaceus*, Appl. Environ. Microbiol. 80 (2014) 5317–5329.

[3] B.L. Cantarel, P.M. Coutinho, C. Rancurel, T. Bernard, V. Lombard, B. Henrissat, The carbohydrate-active EnZymes database (CAZy): an expert resource for glycogenomics, Nucleic Acids Res. 37 (2009) D233–D238.

[4] V. Lombard, H.G. Ramulu, E. Drula, P.M. Coutinho, B. Henrissat, The carbohydrate-active enzymes database (CAZy) in 2013, Nucleic Acids Res. 42 (2014) D490–D495.

[5] D.G. Naumoff, Hierarchical classification of glycoside hydrolases, Biochem. 76 (2011) 622–635.

[6] B. Siguier, M. Haon, V. Nahoum, M. Marcellin, O. Burlet-Schiltz, P.M. Coutinho, B. Henrissat, L. Mourey, M.J. O'Donohue, J.-G. Berrin, S. Tranier, C. Dumon, First structural insights into alpha-L-arabinofuranosidases from the two GH62 glycoside hydrolase subfamilies, J. Biol. Chem. 289 (2014) 5261–5273.

[7] G. Beldman, H.A. Schols, S.M. Pitson, M.J.F. Searle-van Leeuwen, A.G.J. Voragen, Arabinans and arabinan degrading enzymes, in: R.J. Sturgeon (Ed.), Adv. Macromol. Carbohydr. Res, vol. 1, 1997, pp. 1–64 146.

[8] K.M.J. Van Laere, C.H.L. Voragen, T. Kroef, L.A.M. den Broek, G. Beldman, A.G.J. Voragen, Purification and mode of action of two different arabinoxylan arabinofuranohydrolases from *Bifidobacterium adolescentis* DSM 20083, Appl. Microbiol. Biotechnol. 51 (1999) 606–613.

[9] F.J. Contesini, M.V. Liberato, M.V. Rubio, F. Calzado, M.P. Zubieta, D.M. Riaño-Pachón, F.M. Squina, F. Bracht, M.S. Skaf, A.R. Damasio, Structural and functional characterization of a highly secreted α-l-arabinofuranosidase (GH62) from *Aspergillus nidulans* grown on sugarcane bagasse, Biochim. Biophys. Acta - Proteins Proteomics 1865 (2017) 1758–1769.

[10] M.T. Numan, N.B. Bhosle, Alpha-L-arabinofuranosidases: the potential applications in biotechnology, J. Ind. Microbiol. Biotechnol. 33 (2006) 247–260.

[11] P. Kim, Current studies on biological tagatose production using l-arabinose isomerase: a review and future perspective, Appl. Microbiol. Biotechnol. 65 (2004) 243–249.

[12] P. Sánchez-Torres, L. González-candelas, D. Ramón, Expression in a wine yeast strain of the *Aspergillus niger* abfB gene, FEMS Microbiol. Lett. 145 (1996) 189–194.

[13] A.G.J. Voragen, F.M. Rombouts, M.F. Searle-van Leeuwen, H.A. Schols, W. Pilnik, The degradation of arabinans by endo-arabinanase and arabinofuranosidases purified from *Aspergillus niger*, Food Hydrocoll. 1 (1987) 423–437.

[14] B.C. Saha, Alpha-L-arabinofuranosidases: biochemistry, molecular biology and application in biotechnology, Biotechnol. Adv. 18 (2000) 403–423.

[15] H.R. Sørensen, S. Pedersen, A. Viksø-Nielsen, A.S. Meyer, Efficiencies of designed enzyme combinations in releasing arabinose and xylose from wheat arabinoxylan in an industrial ethanol fermentation residue, Enzym. Microb. Technol. 36 (2005) 773–784.

[16] R.M. Berka, I.V. Grigoriev, R. Otillar, A. Salamov, J. Grimwood, I. Reid, N. Ishmael, T. John, C. Darmond, M.-C. Moisan, B. Henrissat, P.M. Coutinho, V. Lombard, D.O. Natvig, E. Lindquist, J. Schmutz, S. Lucas, P. Harris, J. Powlowski, A. Bellemare, et al., Comparative genomic analysis of the thermophilic biomass-degrading fungi *Myceliophthora thermophila* and *Thielavia terrestris*, Nat. Biotech., 29 (2011) 922–927.

[17] Y. García-Huante, M. Cayetano-Cruz, A. Santiago-Hernández, C. Cano-Ramírez, R. Marsch-Moreno, J.E. Campos, G. Aguilar-Osorio, C.G. Benitez-Cardoza, S. Trejo-Estrada, M.E. Hidalgo-Lara, The thermophilic biomass-degrading fungus *Thielavia terrestris* Co3Bag1 produces a hyperthermophilic and thermostable β-1,4-xylanase with exo- and endo-activity, Extremophiles 21 (2017) 175–186.

[18] J.A. Langston, K. Brown, F. Xu, K. Borch, A. Garner, M.D. Sweeney, Cloning, expression, and characterization of a cellobiose dehydrogenase from *Thielavia terrestris* induced under cellulose growth conditions, Biochim. Biophys. Acta - Proteins Proteomics 1824 (2012) 802–812.

[19] A. Margaritis, R.F.J. Merchant, M. Yaguchi, Thermostable Cellulases from thermophilic microorganisms, Crit. Rev. Biotechnol. 4 (1986) 327–367.

[20] F. Segato, A.R.L. Damásio, T.A. Gonçalves, R.C. de Lucas, F.M. Squina, S.R. Decker, R.A. Prade, High-yield secretion of multiple client proteins in *Aspergillus*, Enzym. Microb. Technol. 51 (2012) 100–106.

[21] A.J. Clutterbuck, Sexual and parasexual genetics of *Aspergillus* species, Biotechnology 23 (1992) 3–18.

[22] B.P. Roy, F. Archibald, Effects of Kraft pulp and lignin on *Trametes versicolor* carbon metabolism, Appl. Environ. Microbiol. 59 (1993) 1855–1863.

[23] André R. de LimaDamásio, Tony M. Silva, Fausto B. dos Reis Almeida, Fábio M. Squina, Daniela A. Ribeiro, Adriana F. Paes Leme, Fernando Segato, Rolf A. Prade, João A. Jorge, Hector F. Terenzi, Maria de Lourdes T.M. Polizeli, Heterologous expression of an *Aspergillus niveus* xylanase GH11 in *Aspergillus nidulans* and its characterization and application, Process Biochem. 46 (2011) 1236–1242.

[24] C. Aslanidis, P.J. de Jong, Ligation-independent cloning of PCR products (LIC-PCR), Nucleic Acids Res. 18 (1990) 6069–6074.

[25] W.H. Eschenfeldt, S. Lucy, C.S. Millard, A. Joachimiak, I.D. Mark, A family of LIC vectors for high-throughput cloning and purification of proteins, in: S.A. Doyle (Ed.), High Throughput Protein Expr. Purif. Methods Protoc, Humana Press, Totowa, NJ, 2009, pp. 105–115.

[26] T.C. McIlvaine, A buffer solution for colorimetric comparison, J. Biol. Chem. 49 (1921) 183–186.

[27] G.L. Miller, Use of Dinitrosalicylic acid reagent for determination of reducing sugar, Anal. Chem. 31 (1959) 426–428.

[28] U.B. Ericsson, B.M. Hallberg, G.T. DeTitta, N. Dekker, P. Nordlund, Thermofluor-based high-throughput stability optimization of proteins for structural studies, Anal. Biochem. 357 (2006) 289–298.

[29] T.G.G. Battye, L. Kontogiannis, O. Johnson, H.R. Powell, A.G.W. Leslie, iMOSFLM: a new graphical interface for diffraction-image processing with MOSFLM, Acta Crystallogr. Sect. D Biol. Crystallogr. 67 (2011) 271–281.

[30] G. Winter, xia2: an expert system for macromolecular crystallography data reduction, J. Appl. Crystallogr., 43 (2010) 186–190.

[31] W. Kabsch, Integration, scaling, space-group assignment and post-refinement, Acta Crystallogr. Sect. D Biol. Crystallogr. 66 (2010) 133–144.

[32] P. Evans, Scaling and assessment of data quality, Acta Crystallogr. D. Biol. Crystallogr. 62 (2006) 72–82.

[33] P.R. Evans, G.N. Murshudov, How good are my data and what is the resolution? Acta Crystallogr. Sect. D 69 (2013) 1204–1214.

[34] M.D. Winn, C.C. Ballard, K.D. Cowtan, E.J. Dodson, P. Emsley, P.R. Evans, R.M. Keegan, E.B. Krissinel, A.G.W. Leslie, A. McCoy, S.J. McNicholas, G.N. Murshudov, N.S. Pannu, E.A. Potterton, H.R. Powell, R.J. Read, A. Vagin, K.S. Wilson, Overview of the CCP4 suite and current developments, Acta Crystallogr. Sect. D 67 (2011) 235–242.

[35] A.J. McCoy, R.W. Grosse-Kunstleve, P.D. Adams, M.D. Winn, L.C. Storoni, R.J. Read, Phaser crystallographic software, J. Appl. Crystallogr. 40 (2007) 658–674.

[36] G.N. Murshudov, P. Skubak, A.A. Lebedev, N.S. Pannu, R.A. Steiner, R.A. Nicholls, M.D. Winn, F. Long, A.A. Vagin, REFMAC5 for the refinement of macromolecular crystal structures, Acta Crystallogr. Sect. D 67 (2011) 355–367.

[37] P. Emsley, K. Cowtan, Coot: model-building tools for molecular graphics, Acta Crystallogr. Sect. D 60 (2004) 2126–2132.

[38] V.B. Chen, W.B. Arendall III, J.J. Headd, D.A. Keedy, R.M. Immormino, G.J. Kapral, L.W. Murray, J.S. Richardson, D.C. Richardson, MolProbity: all-atom structure validation for macromolecular crystallography, Acta Crystallogr. Sect. D 66 (2010) 12–21.

[39] E. Krissinel, K. Henrick, Inference of macromolecular assemblies from crystalline state, J. Mol. Biol. 372 (2007) 774–797.

[40] U.K. Laemmli, Cleavage of structural proteins during the assembly of the head of bacteriophage T4, Nature 227 (1970) 680–685.

[41] I. Migneault, C. Dartiguenave, M.J. Bertrand, K.C. Waldron, Glutaraldehyde: behavior in aqueous solution, reaction with proteins, and application to enzyme crosslinking, Biotechniques 37 (2004) 790–802.

[42] T.W. Geders, K. Gustafson, B.C. Finzel, Use of differential scanning fluorimetry to optimize the purification and crystallization of PLP-dependent enzymes, Acta Crystallogr. Sect. F. Struct. Biol. Cryst. Commun. 68 (2012) 596–600.

[43] F.H. Niesen, H. Berglund, M. Vedadi, The use of differential scanning fluorimetry to detect ligand interactions that promote protein stability, Nat. Protoc. 2 (2007) 2212–2221.

[44] M. Vedadi, F.H. Niesen, A. Allali-Hassani, O.Y. Fedorov, P.J. Finerty, G.A. Wasney, R. Yeung, C. Arrowsmith, L.J. Ball, H. Berglund, R. Hui, B.D. Marsden, P. Nordlund, M. Sundstrom, J. Weigelt, A.M. Edwards, Chemical screening methods to identify ligands that promote protein stability, protein crystallization, and structure determination, Proc. Natl. Acad. Sci. 103 (2006) 15835 LP – 15840.

[45] L.E. Kellett, D.M. Poole, L.M. Ferreira, A.J. Durrant, G.P. Hazlewood, H.J. Gilbert, Xylanase B and an arabinofuranosidase from *Pseudomonas fluorescens subsp. cellulosa* contain identical cellulose-binding domains and are encoded by adjacent genes, Biochem. J. 272 (1990) 369 LP – 376.

[46] T. Maehara, Z. Fujimoto, H. Ichinose, M. Michikawa, K. Harazono, S. Kaneko, Crystal structure and characterization of the glycoside hydrolase family 62 α-l-Arabinofuranosidase from *Streptomyces coelicolor*, J. Biol. Chem. 289 (2014) 7962–7972.

[47] A.P. Kaur, B.P. Nocek, X. Xu, M.J. Lowden, J.F. Leyva, P.J. Stogios, H. Cui, R. Di Leo, J. Powlowski, A. Tsang, A. Savchenko, Functional and structural diversity in GH62 alpha-L-arabinofuranosidases from the thermophilic fungus *Scytalidium thermophilum*, Microb. Biotechnol. 8 (2015) 419–433.
[48] M. Mechelke, D.E. Koeck, J. Broeker, B. Roessler, F. Krabichler, W.H. Schwarz, V.V. Zverlov, W. Liebl, Characterization of the arabinoxylan-degrading machinery of the thermophilic bacterium *Herbinix hemicellulosilytica*-Six new xylanases, three arabinofuranosidases and one xylosidase, J. Biotechnol. 257 (2017) 122–130, https://doi.org/10.1016/j.jbiotec.2017.04.023.
[49] R. Pérez, J. Eyzaguirre, Aspergillus fumigatus produces two Arabinofuranosidases from Glycosyl hydrolase family 62: comparative properties of the recombinant enzymes, Appl. Biochem. Biotechnol. 179 (2016) 143–154.
[50] M. Couturier, M. Haon, P.M. Coutinho, B. Henrissat, L. Lesage-Meessen, J.-G. Berrin, *Podospora anserina* hemicellulases potentiate the *Trichoderma reesei* secretome for saccharification of lignocellulosic biomass, Appl. Environ. Microbiol. 77 (2011) 237 LP – 246.
[51] H. Tsujibo, C. Takada, Y. Wakamatsu, M. Kosaka, A. Tsuji, K. Miyamoto, Y. Inamori, Cloning and expression of an α-L-Arabinofuranosidase gene (stxIV) from *Streptomyces thermoviolaceus* OPC-520, and characterization of the enzyme, Biosci. Biotechnol. Biochem. 66 (2002) 434–438.
[52] B.V McCleary, V.A. McKie, A. Draga, E. Rooney, D. Mangan, J. Larkin, Hydrolysis of wheat flour arabinoxylan, acid-debranched wheat flour arabinoxylan and arabino-xylo-oligosaccharides by beta-xylanase, alpha-L-arabinofuranosidase and beta-xylosidase, Carbohydr. Res., 407 (2015) 79–96.
[53] C. Wilkens, S. Andersen, B.O. Petersen, A. Li, M. Busse-Wicher, J. Birch, D. Cockburn, H. Nakai, H.E.M. Christensen, B.B. Kragelund, P. Dupree, B. McCleary, O. Hindsgaul, M.A. Hachem, B. Svensson, An efficient arabinoxylan-debranching alpha-L-arabinofuranosidase of family GH62 from *Aspergillus nidulans* contains a secondary carbohydrate binding site, Appl. Microbiol. Biotechnol. 100 (2016) 6265–6277.
[54] K. Hashimoto, M. Yoshida, K. Hasumi, Isolation and characterization of CcAbf62A, a GH62 α-L-Arabinofuranosidase, from the basidiomycete *Coprinopsis cinerea*, Biosci. Biotechnol. Biochem. 75 (2011) 342–345.
[55] A.P. de Souza, D.C.C. Leite, S. Pattathil, M.G. Hahn, M.S. Buckeridge, Composition and structure of sugarcane Cell Wall polysaccharides: implications for second-generation bioethanol production, BioEnergy Res. 6 (2013) 564–579.
[56] B.A. Katz, A. Kossiakoff, The crystallographically determined structures of atypical strained disulfides engineered into subtilisin, J. Biol. Chem. 261 (1986) 15480–15485.
[57] B. Schmidt, L. Ho, P.J. Hogg, Allosteric disulfide bonds, Biochemistry 45 (2006) 7429–7433.
[58] M. Paoli, An elusive propeller-like fold, Nat. Struct. Biol. 8 (2001) 744.
[59] M.J. Bennett, S. Choe, D. Eisenberg, Domain swapping: entangling alliances between proteins, Proc. Natl. Acad. Sci. U. S. A. 91 (1994) 3127–3131.
[60] M.J. Bennett, M.P. Schlunegger, D. Eisenberg, 3D domain swapping: a mechanism for oligomer assembly, Protein Sci. 4 (1995) 2455–2468.
[61] A.M. Gronenborn, Protein acrobatics in pairs – dimerization via domain swapping, Curr. Opin. Struct. Biol. 19 (2009) 39–49.
[62] Y. Liu, D. Eisenberg, 3D domain swapping: as domains continue to swap, Protein Sci. 11 (2002) 1285–1299.
[63] F. Rousseau, J.W.H. Schymkowitz, L.S. Itzhaki, The unfolding story of three-dimensional domain swapping, Structure 11 (2003) 243–251.
[64] L. Holm, P. Rosenström, Dali server: conservation mapping in 3D, Nucleic Acids Res. 38 (2010) W545–W549.
[65] X. Robert, P. Gouet, Deciphering key features in protein structures with the new ENDscript server, Nucleic Acids Res. 42 (2014) W320–W324.
[66] T. Tonozuka, Y. Tanaka, S. Okuyama, T. Miyazaki, A. Nishikawa, M. Yoshida, Structure of the catalytic domain of alpha-L-Arabinofuranosidase from *Coprinopsis cinerea*, CcAbf62A, provides insights into structure-function relationships in glycoside hydrolase family 62, Appl. Biochem. Biotechnol. 181 (2017) 511–525.
[67] O.V. Moroz, L.F. Sobala, E. Blagova, T. Coyle, W. Peng, K.B.R. Morkeberg Krogh, K.A. Stubbs, K.S. Wilson, G.J. Davies, Structure of a *Talaromyces pinophilus* GH62 arabinofuranosidase in complex with AraDNJ at 125 A resolution, Acta Crystallogr. Sect. F 74 (2018) 490–495.
[68] T. Pons, D.G. Naumoff, C. Martinez-Fleites, L. Hernandez, Three acidic residues are at the active site of a beta-propeller architecture in glycoside hydrolase families 32, 43, 62, and 68, Proteins 54 (2004) 424–432.
[69] J.W. Schymkowitz, F. Rousseau, H.R. Wilkinson, A. Friedler, L.S. Itzhaki, Observation of signal transduction in three-dimensional domain swapping, Nat. Struct. Biol. 8 (2001) 888–892.
[70] S. Yang, H. Levine, J.N. Onuchic, Protein oligomerization through domain swapping: role of inter-molecular interactions and protein concentration, J. Mol. Biol. 352 (2005) 202–211.
[71] S. Bershtein, W. Mu, E.I. Shakhnovich, Soluble oligomerization provides a beneficial fitness effect on destabilizing mutations, Proc. Natl. Acad. Sci. 109 (2012) 4857 LP – 4862.
[72] E. Folta-Stogniew, Oligomeric States of Proteins Determined by Size-Exclusion Chromatography Coupled with Light Scattering, Absorbance, and Refractive Index Detectors, in: New Emerg, Proteomic Tech., Humana Press, Totowa, NJ, 2006, pp. 97–112.